Pergamon

Carbon, Vol. 32, No. 2, pp. 289–299, 1994

0008-6223/94 $6.00 + .00

FIRST-PRINCIPLES STUDY OF THE STACKING EFFECT ON THE ELECTRONIC PROPERTIES OF GRAPHITE(S)

J.-C. CHARLIER, X. GONZE, and J.-P. MICHENAUD
Laboratoire de Physico-Chimie et de Physique des Matériaux, Université Catholique de Louvain, 1, Place Croix du Sud, B-1348 Louvain-La-Neuve, Belgium

(*Received* 26 *July* 1993; *accepted in revised form* 23 *August* 1993)

Abstract—In this paper, we present a thorough *ab initio* study of different forms of graphite. The interplanar distance and the electronic properties of different stackings of graphene sheets (simple hexagonal {AAA. . .}, hexagonal {ABAB. . .} and rhombohedral {ABC. . .} graphites) have been studied in the framework of the density functional theory. The valence charge densities and the densities of states of these three graphitic structures are presented and compared, as well as their respective band structures. As graphite possesses a semimetallic behavior, the overlap between conduction and valence bands has been investigated in function of the stacking. *Ab initio* results are related to experimental data obtained for *natural* graphite. *Tight-binding* Fermi surfaces are also presented in order to discuss the sensitive electronic behavior of graphite near the Fermi level.

Key Words—Graphite, allotropic forms, electronic properties, structural properties, density functional theory.

1. INTRODUCTION

At ordinary temperatures and pressures, the stable form of carbon is graphite, a semimetallic form without any analog in the group IV series. *Natural* graphite occurs in two crystal structures: the Bernal [1] and the rhombohedral[2] structures. Samples usually contain no more than 5–15% of rhombohedral structure intermixed with the Bernal form and disordered graphite[2,3]. A third geometrical possibility consists in simple hexagonal graphite, similar to the arrangement of carbon atoms found in certain graphite intercalation compounds (GICs) such as (LiC_n)[4]. Crystals of almost pure hexagonal graphite, also called highly oriented pyrolitic graphite (HOPG)[5] can be made by high temperature heat treatment and quenching, but the pure rhombohedral and simple hexagonal forms have never been isolated. Moreover, disordered graphitic forms[6], like pregraphitic carbon and turbostratic graphite where random rotation and translation of the graphene sheets appear, can also be found in the nature.

All of these forms of graphite consist of planes of carbon atoms each forming a hexagonal net with a well-established nearest-neighbor distance of 1.42 Å, stacked with an interplanar spacing around 3.35 Å. However, they differ in the stacking sequence of the carbon planes. Simple hexagonal graphite has an AAA-stacking with all carbon atoms in consecutive layers located directly on top of each other. The Bernal structure possesses an ABAB-stacking, with half of the atoms directly above each other in adjacent planes and the other half directly above the center of the hexagonal ring in the adjacent plane. Rhombohedral graphite has an ABC-stacking, with half of the atoms directly below atoms in the adjacent plane and directly above hexagonal ring centers and the other half of the atoms directly above atoms and below hexagonal ring centers (Fig. 1). The transition path between these structures can be obtained by slipping one {AAA → ABAB} or two {AAA → ABC; ABAB → ABC} entire graphene sheets by a 1.42 Å or 2.84 Å distance in the C-C bond direction, as shown in Fig. 1.

Many calculations have been devoted to graphite[7]. In 1947, P. R. Wallace[8] proposed a tight-binding model for the electronic properties of 2D-graphite. The graphene sheet was found to be a zero-gap semiconductor. In 1955, extending the two-dimensional model of Wallace for the graphite lattice to the three-dimensional lattice by a -k.p-perturbation calculation, J. C. Slonczewski and P. R. Weiss[9] proposed a semimetallic behavior for 3D-graphite. They analysed some general features of the structure of the π bands in the neighborhood of the Brillouin zone edge and expressed them in terms of interatomic parameters (γ_i). The same year, using the de Haas–van Alphen effect in the magnetic susceptibility of graphite, J. W. McClure[10] gathered information concerning the π band structure (total overlap, energy differences, γ_i parameters evaluation . . .) and constructed a first model of Fermi surface for pure graphite composed of a central hole pocket surrounded by two electron ones (unlike modern studies[11]), submitted to an anisotropic trigonal warping (γ_3). These two last works form the well-known Slonczewski–Weiss–McClure model [SWMcC].

All of the above calculations assume that graphite crystallizes in the Bernal[1] structure. In 1958, R. R. Haering[3] investigated the band structure of rhombohedral graphite using the nearest-neighbor tight-binding approximation. An extension of Haering's calculation including the interaction between

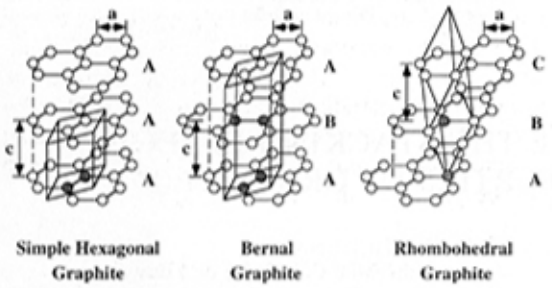

Simple Hexagonal Graphite | Bernal Graphite | Rhombohedral Graphite

Fig. 1. Comparison between three different graphitic structures: simple hexagonal, hexagonal (Bernal), and rhombohedral graphites. They differ in the shift imposed on the middle plane in the ABAB-stacking, on all planes in the ABC-stacking, while all the planes are directly above each other in the AAA-stacking. The unit cells which belongs to the hexagonal {AAA and ABAB} and rhombohedral symmetries {ABC} are also shown in the different structures with their respective number of incorporated carbon atoms (grey). The interlayer distance is c, and the distance between nearest-neighbors is a.

nearest neighboring planes was proposed 10 years later by J. W. McClure[12]. The semimetallic behavior was also found for this new allotropic form.

In 1965, in order to agree with more precise experimental data, G. Dresselhaus and M. S. Dresselhaus[13] refined, using group theory, a new model for Bernal graphite including spin orbit interaction, which explained small departures from the usual SWMcC model.

In 1967, F. Bassani and G. Pastori Parravicini[14] applied a *semi-empirical method* using a *tight-binding* approach to compute an accurate graphite band structure in agreement with the semimetallic behavior of graphite, already proposed in the analytical SWMcC model.

Since the 1970s, many *ab initio* studies, where matrix elements of the Hamiltonian are calculated directly without any *tight-binding* approximations (or any other *a priori* assumptions), have been devoted to graphite band structure calculation or/and SWMcC interaction parameters evaluation[15]. Details of the band structures became more and more accurate as a function of the year of the publication of the study. In these simulations, graphite has often been investigated either as the archetypal two-dimensional solid due to its strongly anisotropic layered structure, or in order to consider the efficiency of a new calculation method.

Since then, some *ab initio* studies have also included the structural properties of 2D-graphite[16] and 3D-graphite[17] by evaluating lattice parameters (in-plane constant and interlayer spacing), cohesive energy, bulk modulus, force constants, compressibility. . . .

In 1986–87, S. Fahy *et al.* proposed two interesting studies dedicated to the transition between rhombohedral graphite and diamond[18] and between simple hexagonal graphite and hexagonal diamond[19].

Even today, the electronic structure of graphite(s) presents a challenge for solid-state theory because of the presence of the two distinct types of interatomic bonding[20–22]. We aim at presenting state-of-the-art *ab initio* calculations of a whole set of electronic properties—valence charge densities, band structures, densities of states (DOS) for these three graphitic structures—and to examine more precisely the effect of the stacking on such properties.

The paper starts with a critical discussion of the *ab initio* theoretical method (Sec. 2), a self-consistent density-functional approach, using *ab initio* nonlocal pseudopotentials and a local-density approximation for exchange and correlation. It is followed by a presentation of the *ab initio* graphitic structures (Sec. 3). Numerical results for the electronic properties of the three structures of graphite are presented and discussed in sections 4 and 5. Finally, we summarize this study.

We hope that our comparative study of the three allotropic forms of graphite can lead to a first step for the qualitative resolution of the electronic properties of the turbostratic graphite (pregraphitic carbon)[23], which is another modification of graphite without any periodicity in the direction perpendicular to the planes of hexagonally arranged carbon atoms. This work can also stimulate future experimental work relative to the electronic properties of GIC where *rigid band models* are often used. Last, the understanding of the physical properties of different types of graphites has been found relevant for the study of the multilayered versions of the recently discovered cylindrical forms of carbon (multilayered nanotubes)[24].

2. THEORETICAL METHOD

The theoretical method used in the present note is similar to the method used in our previous published studies[20,21]. We performed a quite standard Hohenberg–Kohn–Sham density-functional calculation (DFT)[25] with the Ceperley–Alder exchange–correlation energy (LDA) as parametrized by Perdew and Zunger[26]. The ionic-core potential of carbon nucleus which is surrounded by two core electrons and four valence electrons, $(1s^2)\ (2s^2\ 2p^2)$, has been replaced by an *ab initio* norm-conserving pseudopotential, which was constructed using the same procedure as in the work of Bachelet, Hamann, and Schlüter[27], but with different "ccl parameters": 1.8 ($l = 0$), 2.0 ($l = 1$), and 3.5 ($l = 2$). The transferability of this pseudopotential has also been tested.

We used a plane wave basis set (up to 1700 plane waves, depending on the required accuracy) within the framework fo the momentum-space formalism[28] and solved the self-consistent Schrödinger equation for the band structure, using the algorithm of Wood and Zunger[29] and a modified "simple-mixing" scheme[30] for the density self-consis-

tency. Special k points[31] were used to sample of the Brillouin zone. For each graphite study, we carefully checked the Brillouin zone sampling and the number of plane waves, in order to get maximum truncation error on energies on the order of 5 meV.

3. *AB INITIO* GRAPHITES

The unit cells of the simple hexagonal, hexagonal, and rhombohedral graphites belong, respectively, to the P6/mmm space group (D^1_{6h}), $P6_3/mmc$ space group (D^4_{6h}), and $R\bar{3}m$ (D^5_{3d}) and contain two, four, and two atoms (Fig. 1).

In graphite, the spacing between layers is large compared with the C-C bond-length distance in the layers. At zero Kelvin, the distance between nearest-neighbors a is 1.42 Å. The interlayer separations c, calculated by minimizing the total energy obtained by the theoretical method, are 3.335 Å {AAA . . .}, 3.35 Å {ABAB . . .}, and 3.34 Å {ABC . . .}, respectively. These calculated values for equilibrium c-axis lattice constant are in good agreement with the experimental 4.2 K value (3.337 Å) obtained for *natural* graphite[32]. The most stable phase (minimum of total energies) is hexagonal graphite. The total energies of the two other forms are respectively greater, by 0.11 meV/atom for rhombohedral graphite and by 17.31 meV/atom for simple hexagonal graphite.This difference explains the presence of rhombohedral phase mixed with hexagonal one in *natural* graphite and the absence of simple hexagonal phase in unconstrained graphite.

These ab initio results confirm that the interplanar binding in graphite is well described by calculations relying on the LDA (Sect. 2), which does not describe properly the long-range behavior of the exchange-correlation potential (image charge and dynamical dipole–dipole interaction). The interplanar forces, which are commonly attributed to van der Waals interactions, actually arise, at least partially, from the overlap of semifilled occupied p_z orbitals (π) perpendicular to the three hybridized σ orbitals[22]. A careful analysis of the interplanar interaction in graphite using the LDA approximation will be published in a forthcoming paper[33].

4. ELECTRONIC PROPERTIES

4.1 Ab initio *valence charge densities*

The valence charge densities of the three crystalline graphites have been calculated using the *ab initio* technique described in the theoretical section, with *ab initio* crystalline parameters for the interplanar distance c. In these investigations, a maximum kinetic energy of 64 Ry {AAA: 989 plane waves, ABAB: 2*995 plane waves, ABC: 993 plane waves} and 28 special k points have been used to obtain the respective self-consistent density.

The isodensity lines are presented in Fig. 2. They display the main features of binding: the *quite weak* bonds in the plane (110) perpendicular to the graphitic layers (upper part) relative to the covalent ones between carbon atoms in the plane (001) (lower part). The hexagonal symmetry is shown up in the in-plane density, while the c-axis density exhibits the absence {AAA} or the presence {ABAB & ABC} of shift between neighboring planes in the stacking. The anisotropy of these crystals is obvious, and these stackings of carbon planes explain the easy cleavage of these materials.

4.2 Ab initio *band structures*

The self-consistent calculations of the densities of charge allows us to construct the respective Kohn–Sham band structures using a set of plane waves leading to a kinetic energy of 72 Rydbergs.

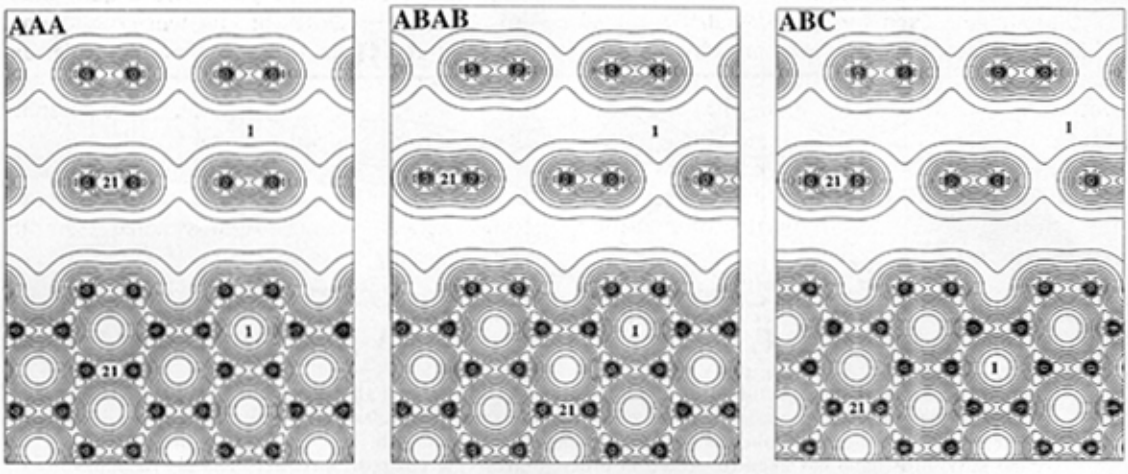

Fig. 2. Self-consistent valence electron pseudocharge densities of simple hexagonal, Bernal, and rhombohedral graphites. The density (up) perpendicular to graphitic planes (110) is directly connected to the density (down) in the graphitic plane (001). The contour interval is in units of 0.1 electrons/(Å)^3 with a difference of 0.2 electrons/Å)^3 between curves.

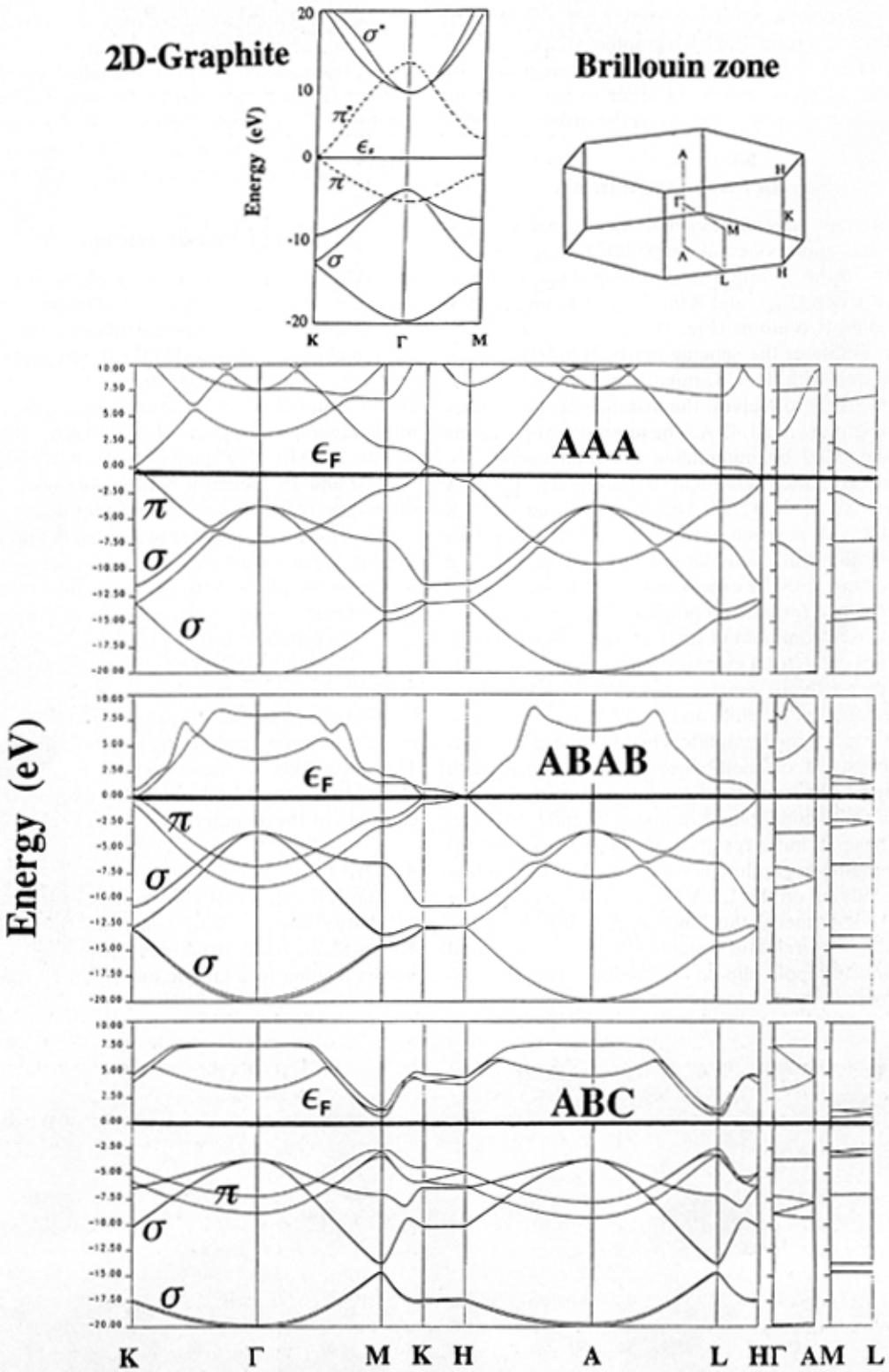

Fig. 3. *Ab initio* band structures of simple hexagonal, Bernal, and rhombohedral graphites along different lines in the hexagonal Brillouin zone. For the sake of comparison, this Brillouin zone has been imposed on the rhombohedral structures using a 6-atom unit cell. The length scales of the three band structures have not been respected in order to make the comparison easier. The 2D graphite band structure (data extracted from Zunger[16]) and the hexagonal Brillouin zone showing several high symmetry points are also presented (top). Each symetrical point is labeled with the usual Bouckaert–Smoluchowski–Wigner notation[42] (Γ,A,H,K,L,M). The σ and π bands and the Fermi level ε_F are labeled in the different band structures.

Table 1. Characteristic electronic energies (in eV) of simple hexagonal, Bernal, and rhombohedral graphites evaluated from the Fermi level at the Γ point. The first three columns are our theoretical results. The last column is a collection of experimental data relative to *natural* graphite

	AAA	ABAB	ABC	Experiment
Bottom σ	−19.5	−19.8	−19.8	
		−20.1	−19.8	−20.6[a]
			−20.1	
Bottom π	−6.6	−6.8	−7.2	−7.2[a], −6.6[b], −5.7[c]
		−8.9	−8.8	−8.1[a], −8.5[b]
			−8.8	
Top σ	−3.1	−3.5	−3.6	−4.6[a], −5.5[b]
		−3.4	−3.7	
			−3.7	
Unoccupied σ^*	3.9	3.7	3.3	
	8.2	7.9	7.6	6.9[a]
		7.9	7.6	

[a]W. Eberhardt, J. T. McGovern, E. W. Plummer, and J. E. Fischer, *Phys. Rev. Lett.* **44,** 200 (1980).
[b]A. R. Law, J. J. Barry, and H. P. Hughes, *Phys. Rev.* B **28,** 5332 (1983).
[c]A. Bianconi, S. B. M. Hagström, and R. Z. Bachrach, *Phys. Rev.* B **16,** 5543 (1977).

Fig. 3 shows the band structures of the three graphitic stackings in different special directions of the Brillouin zone shown in the insert. For the sake of comparison, we have chosen to work with a hexagonal Brillouin zone for every form, thus using a 6-atom unit cell for rhombohedral graphite. As the three allotropic forms of graphite possess a different number of carbon atoms (simple hexagonal: 2, hexagonal: 4, rhombohedral: 6) in the *hexagonal* unit cell, the numbers of valence bands are respectively 4 {AAA}, 8 {ABAB}, and 12 {ABC}.

In graphite, the strong bonding (angles of 120° between the segments connecting nearest-neighbor atoms) within the layers (intralayer) is described by sp^2 hybridized 2s, $2p_x$, and $2p_y$ atomic orbitals (σ states), and the weak interlayer bonding is derived from the overlap between $2p_z$ orbitals (π states) perpendicular to the graphitic planes. The resulting band structure consists of bonding π and σ states and antibonding π^* and σ^* states forming the valence and conduction bands, respectively. The weak interactions between graphitic planes modify the 2D-situation (which leads to a zero-gap semiconductor[8]) and create a small or wide overlap semimetal, depending on the allotropic structure.

The band structures of these three forms of graphite, dominated by these two-dimensional in-plane interactions, are expected to be nearly identical. The main features of the energy bands of graphite are directly obtained with a good accuracy using a two-dimensional calculation, except for the energy range close to the Fermi energy (ε_F). The electronic and transport properties are governed by this region where the three structures differ significantly from each other. The aim of the next section is to find these important differences in the π-bands close to the Fermi energy.

Our *ab initio* calculations demonstrate the essentially two-dimensional (2D) character of the three structures by predicting little or no dispersion of the σ bands perpendicular to the basal planes, although the π bands show some c-axis dispersion. In the AHL plane of the Brillouin zone of the AAA and ABAB forms, the tridimensional structure is very similar to the monolayer band structure also presented in Fig. 3. The crystallographic structures possess a twofold screw axis normal to the zone boundary plane[34], imposing a degeneracy not to be lifted to any order over the entire plane. By contrast, the middle plane ΓMK of the Brillouin zone does not possess such a particular reversal element, and some degeneracies are lifted. This lift of the degeneracy is nearly invisible in Fig. 3, but lines KH, ΓA, and ML show some more strongly lifted degeneracies. At the Γ point, the dispersions of the π bands are also very strong.

Table 1 focuses on AAA, ABAB, and ABC electronic energies and compares them to experimental values for *natural* graphite.

In general, the present results are consistent with experimental data. The effect of the stacking on the main features of the band structures is very weak. The total valence band width {AAA: 19.5 eV, ABAB: 20.1 eV, ABC: 20.1 eV}, the σ-band width {AAA: 16.4 eV, ABAB: 16.7 eV, ABC: 16.5 eV}, and the σ-π band separations {AAA: 12.9 eV (bottom) and 3.5 eV (top), ABAB: 10.9 eV (bottom) and 3.3 eV (top), ABC: 11.3 eV (bottom) and 3.6 eV (top)} are very close to each other. A large difference between theoretical and experimental results appears for the eigenvalues at the top of the σ band, but this is in agreement with recent pseudopotential calculations[22]. As the σ orbitals are more compact than the π orbitals, incomplete cancellation of the

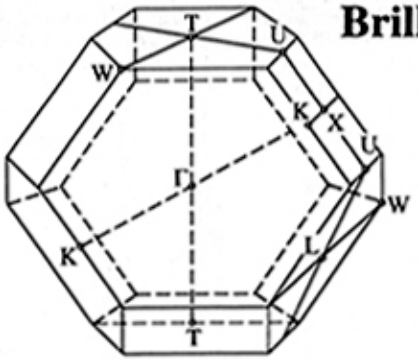

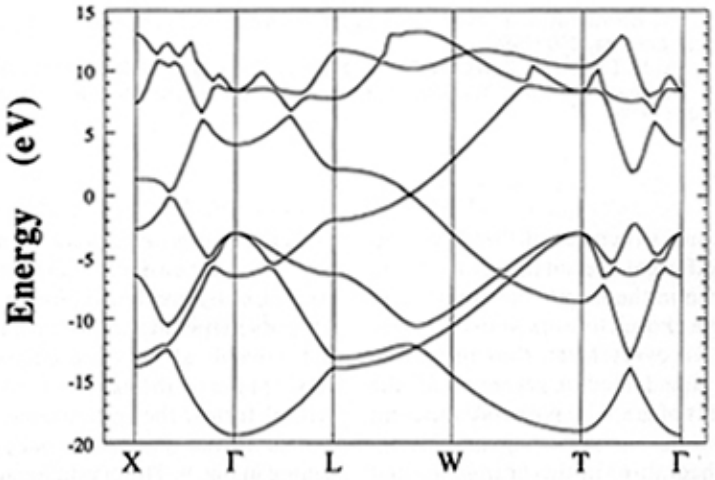

Fig. 4. *Ab initio* band structure of rhombohedral graphite along different lines in the rhombohedral Brillouin zone, which is also presented showing several high symmetry points (Γ,T,L,X,W,K,U). A crossing point can be found along the L–W line and an avoided crossing along Γ–X.

Hartree self-interaction in the LDA will raise the energy of the σ bands with respect to the π bands as proposed by Schabel *et al.*

Although the band structure of rhombohedral graphite calculated along different special lines of the hexagonal Brillouin zone would lead to an insulating behavior for this material (Fig. 3), a *crossing point* coming from a degeneracy line appears along the L–W line of the rhombohedral Brillouin zone (Fig. 4). In fact, this degeneracy line is so localized that the associated semimetallic behavior (easily obtained for the two other allotropic forms) only appears, in this case, when using a localized set of k-points.

4.3 Ab initio *densities of states*

The electronic densities of states (DOS) have been calculated with the tetrahedron method[35], using, respectively, 198 k points for the AAA and ABAB-stackings in the hexagonal Brillouin zone and 946 k points for the ABC-stacking in the rhombohedral Brillouin zone and a kinetic energy of 72 Rydbergs associated to the set of plane waves ($\pm$1700). The calculated DOS for the valence states of these three graphites are presented in the Fig. 5.

The bidimensional characteristic of the first σ bands, which had already been seen in the lack of dispersion along the K-H, Γ-A, and M-L lines in the band structure, is confirmed by the characteristic step function that appears in the DOS form of each graphite. The nearly constant value, displaying a 2D-behavior, stands between -20 eV and -13 eV. The small oscillations around this constant value should be ascribed to the tetrahedron method[36]. In the energy interval $[-13; 0]$ eV, the other σ bands and the π bands, which overlap near the Γ point, are responsible for the main features. The comparison of the three graphitic cases reflects the quite good reproduction of the peak locations.

As the electronic nature of a structure (semiconducting, semimetallic, or metallic) depends on the density of states in the region of the Fermi level[23], the theoretical overlap value is presented in each respective DOS of the Fig. 5. Simple hexagonal and Bernal graphites possess overlaps of 1.6 eV and 28 meV, respectively. Although the rhombohedral

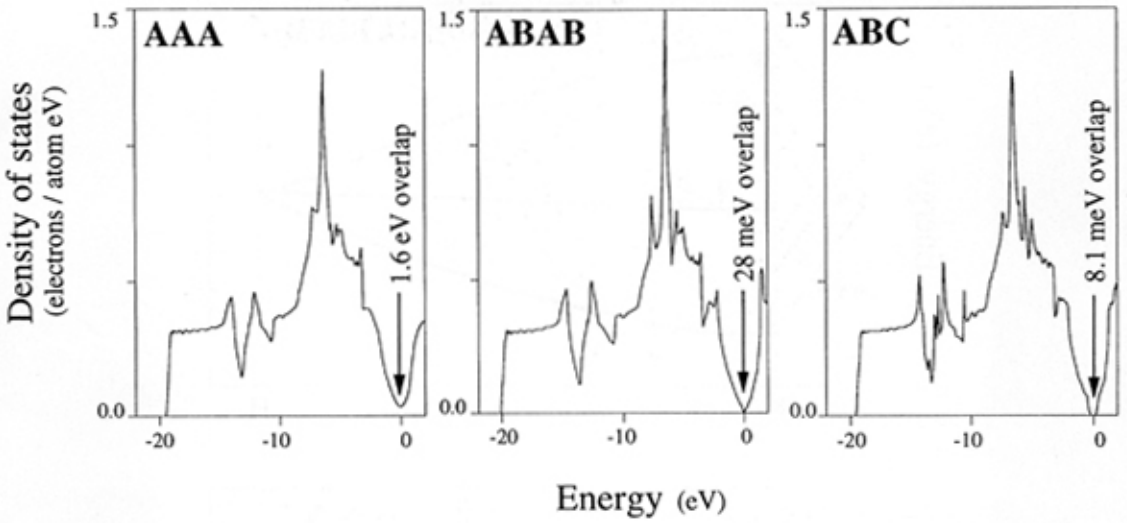

Fig. 5. Densities of states (DOS) of simple hexagonal, Bernal, and rhombohedral graphites. The *ab initio* value of the overlap is presented in the respective DOS.

graphite DOS shown in Fig. 5 presents a small direct gap (0.29 eV) using the 946 k points sampling, a careful examination of the band structure near the conduction-band minimum and the valence-band maximum, using a very fine mesh of k points localized in a region that lies close to the HKH hexagonal Brillouin zone boundary, leads to the conclusion that ABC graphite is actually a semimetal with a very small overlap of 8.1 meV. With the 946 k points sampling (already larger than for the two other forms), it is not possible to distinguish reliably between a semimetal with a small overlap and a semiconductor with a small gap due to the locality of this weak effect, which will be extensively explained in the next section.

5. DISCUSSION

As already mentioned, a single isolated graphene sheet is a zero-gap semiconductor (or zero-overlap semimetal) due to the phase relations of the Bloch state at the K-point of the 2D Brillouin zone (Cfr. Fig. 3). The states near the overlap in any of the stackings {AAA, ABAB, or ABC} of graphite are made up from these Bloch states.

To a first approximation, the π-bands near K in Bernal graphite contain two distinct types of state: (a) those made up from p_z-states of carbon atoms that have atoms directly above and below them in the neighboring graphite layers, and (b) those made from p_z-states of atoms with centers of hexagonal rings above and below them. Because of the phase relations of Bloch states at K of type (b), there is no interaction between these states and the neighboring graphite layers; the interaction that causes the 28 meV dispersion (40 meV in exp.[37]) along the *c*-axis (K–H line) is a second-nearest-layer interaction, giving that very flat band, presented in Fig. 6, which determines the Fermi surface of hexagonal graphite in a very delicate way as presented in Fig. 7. This *tight-binding* Fermi surface that is in agreement with ab initio Fermi surface[20] is composed of two pockets of holes surrounding one pocket of electrons centered in K and possesses a trigonal axis along the HKH edge of the Brillouin zone due to the γ_3 parameter of the Slonczewski–Weiss–McClure (SWMcC) model[9,10].

The 28 meV ($2|\gamma_2|$) overlap is basically governed by a -14 meV matrix element γ_2 between states on second-nearest-layers of graphite of the SWMcC model (Cfr. Fig. 6). The matrix-element γ_1 for nearest-layer states is on the order of 0.36 eV, and it is only the special symmetry of the K state that prevents this matrix element from coming into play[38]. The states of type (1) show a dispersion of about 1.6 eV ($4\gamma_1$) along the K-H line (Cfr. Fig. 6), as expected, because the symmetry of the K state does not remove the nearest-layer interaction for them.

In simple hexagonal graphite, there are only states of type (1), so the dispersion in the *c*-direction of about 1.6 eV ($4\alpha_1$ where $\alpha_1 \approx \gamma_1$)[39] gives the calculated overlap for AAA-stacking graphite[21] (Cfr. Fig. 6). The corresponding *tight-binding* Fermi surface (Fig. 7) is also in good agreement with the *ab initio* one. However, in contrast to the Bernal surface, an inversion in the nature of the carriers is found, and the Fermi surface is now composed of a hole pocket centered at the K point and one electron pocket centered at the H point of the Brillouin zone and does not possess trigonal symmetry any more (no corresponding to the γ_3 parameter in this model).

In rhombohedral graphite, the situation is a little different. Each atom has either one atom directly above it and no atom directly below it (in the neighboring layers), or vice versa.

Considering the two atoms directly above and below each other in neighboring layers, if these two

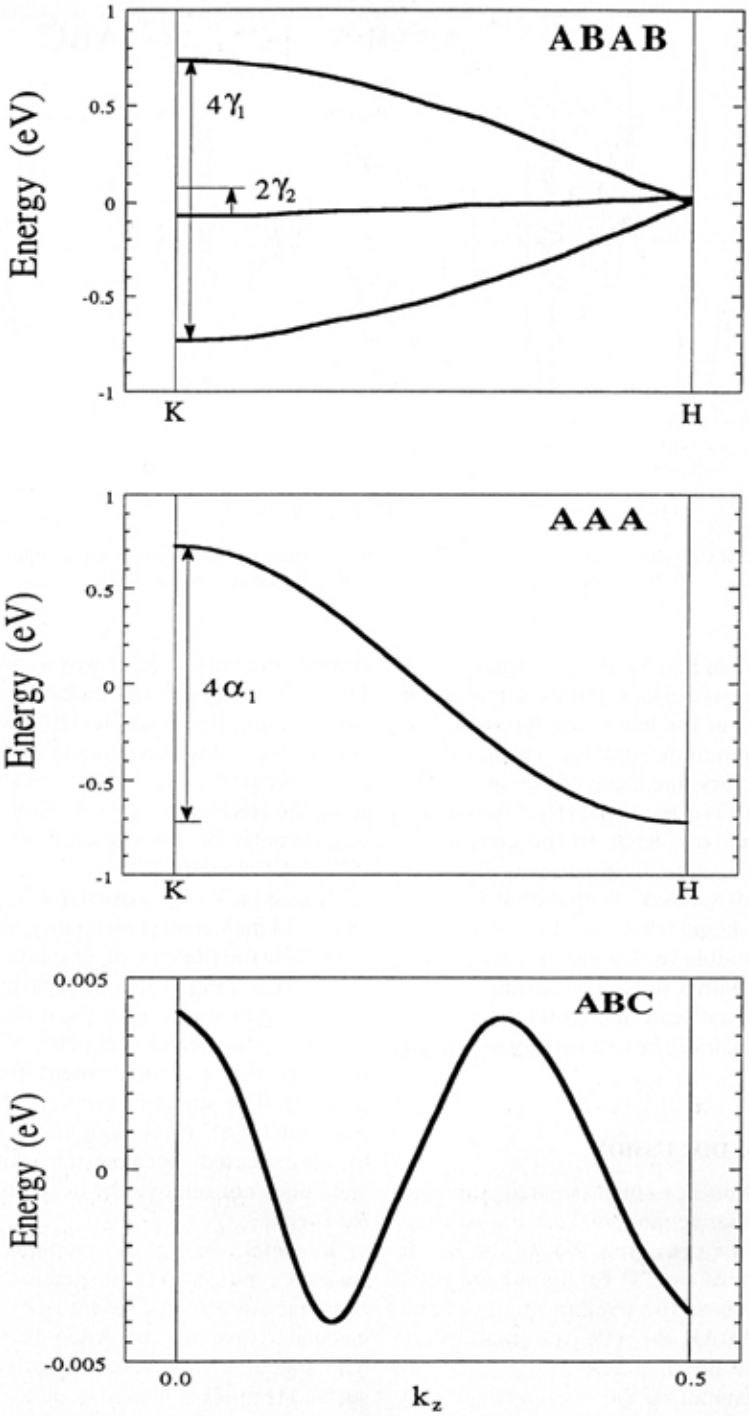

Fig. 6. Band structure of simple hexagonal, Bernal, and rhombohedral graphites detailed around the Fermi level in the interval [−1.0;1.0] eV along K–H line of the hexagonal Brillouin zone for the two first allotropic forms and along k_z axis for the last one. These band structures show the different graphitic overlaps and certain interaction parameters (γ_1,γ_2,α_1) coming from the respective *tight-binding* models [39],[9,10],[3,12]. Note that the abscissae axes are in arbitrary units, and the scales do not correspond.

layers were completely isolated, there would be a bonding and antibonding combination, split by about 1–1.6 eV. As we move away from the K point (in the 2D Brillouin zone) each of these combinations splits (by interaction with nearest-neighbor in the same layer), giving the bonding and antibonding π-bands. The bonding and antibonding π-bands will cross at some distance (in k-space) from the K point, to give a zero-gap semiconductor (as in ABAB stacking). As predicted by group theory, this cross-

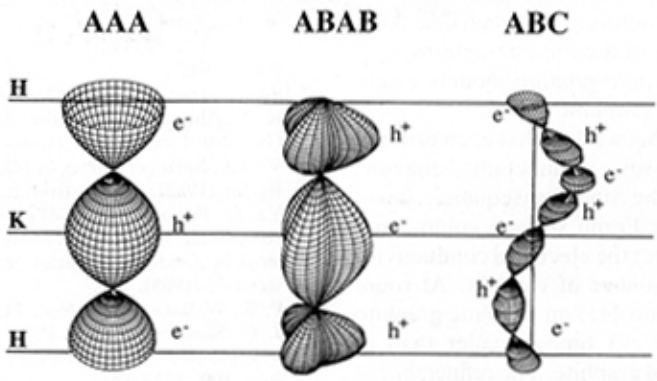

Fig. 7. Tridimensional *tight-binding* Fermi surface of simple hexagonal, Bernal, and rhombohedral graphites in agreement with the three respective *tight-binding* models [39],[9,10],[3,12]. All of the three Fermi surfaces are centered on one of the six vertical edges HKH of the hexagonal Brillouin zone. To be comparable, the length of this edge has been adjusted to the same value for each graphite. The electron and hole pockets are labeled by e^- and h^+ respectively. The widths of the surfaces of hexagonal and rhombohedral graphites have been magnified by several orders of magnitude (in arbitrary units).

ing of bands is dictated by *symmetry*. The degeneracy line is presented in Fig. 6, showing the little overlap (8.1 meV) due to the dispersion along the k_z-direction of the degenerated conduction–valence bands produced by the second-layer interaction. This *c*-axis dispersion along the degeneracy line, which gives a very small overlap semimetal, has been discussed in the Haering–McClure model[3,12] where the two π bands still touch, as they do in 2D-graphite, but this touching does not occur at points of special symmetry of the zone, but lies on cylinders whose axes are the edges.

In Bernal graphite, the crystal symmetry forces a degeneracy of the valence and conduction bands at special points on the six vertical edges of the Brillouin zone, and the dispersion of these bands along these edges gives rise to the Fermi surface. In this particular case, the zero-gap is dictated *by high symmetry* in the absence of second-layer interactions. In rhombohedral graphite, the symmetry, which forces the existence of a Fermi surface and causes degeneracy to occur in the two-band model, does not localize these effects on special symmetry points. The small overlap in ABC graphite spirals around the HKH edge of the Brillouin zone at a very short distance away, the *tight-binding* Fermi surface shown in Fig. 7 is composed of three-hole and three-electron pockets also spiraling around this boundary line. The comparison between our result and the touching bands model of McClure is in total agreement, in spite of the approximations in McClure's description[12].

Before the present calculation, S. Fahy *et al.*[18], in their own LDA calculation, had obtained a direct band gap of 0.05 eV. Although they calculated the band structure on a very fine mesh in the region of the valence-band maximum and the conduction-band minimum, they missed the overlap. This could be explained[40] by the use of a set of localized orbitals, which cannot demonstrate the very delicate interplay between the in-layer matrix elements and the second-nearest-layer matrix elements. The width of the Fermi surface (number of carriers) is very sensitive to the stacking of the graphene sheets. This point is of general significance for pure graphite because it is experimentally observed that in pregraphitic carbon (turbostratic graphite), where the layers are well formed but their stacking is poorly characterized, graphite still behaves as a semimetal[41]. This result could be explained by a combination of the electronic nature of the different ordered stackings as already discussed in a previous work[23].

6. CONCLUSION

A self-consistent total energy study has been performed for the interlayer spacing of the different allotropic forms of graphite. These calculations are found to be in good agreement with experimental data relative to *natural* graphite and confirm that the bonding between graphene sheets is not uniquely dominated by van der Waals dispersive interactions. The overlap between the p_z orbitals perpendicular to the graphene sheets is accurately simulated by the DFT+LDA method[33].

The electronic properties of simple hexagonal, Bernal, and rhombohedral graphites have been compared, leading to a theoretical understanding of the effect of the stacking. The band structures of graphites have been analyzed and compared to the bidimensional case. The DOS have also been investigated, and a comparison of DOS has revealed similar 2D-character for the first σ bands at the Γ point, which entails a step function in a part of each DOS. In the three allotropic forms, band structure and DOS confirm that graphite possesses a semimetallic behavior and that the overlap value depends on the stacking position of its graphene sheets. The Fermi

surfaces in the three structures have been discussed and explained in terms of atomic interactions relative to the respective *tight-binding* models established for the different graphitic forms.

The main result of this work is that each ordered form of graphite possesses a semimetallic behavior, and modifications of the stacking sequence introduce a variation of the Fermi surface volume and in turn significantly affect the electrical conductivity due to the different number of carriers. At room temperature, observations[41] on pyrolitic graphite display a conductivity ~3 times smaller than in single-crystal hexagonal graphite. The refinement of the Fermi surface that appears in the transition path between AAA → ABAB → ABC, leading to a lower carrier concentration in the pyrolitic form added to the shorter mean free path due to a higher concentration of scattering defects in such crystal, are possible explanations for this phenomenon.

At last, this study displays that the present method (DFT+LDA) of band structure calculation is a powerful tool in a theoretical investigation of many physical properties of layered-type crystals with well pronounced anisotropic charge distribution, requiring accurate resolution of meV energy differences.

Note added in proof. By increasing the number of k-points from 28 to 40 in the irreductible part of the Brillouin zone (see section 4.1), we have observed that the c optimal value of simple hexagonal graphite was changed from 3.335 Å to 3.66 Å.

This more accurate sampling does not affect the c-axis lattice parameter of the two other forms of graphite as well as the electronic properties of simple hexagonal graphite at the c = 3.335 Å lattice parameter value.

Acknowledgements—We thank S. Fahy, M. S. Dresselhaus, G. Dresselhaus, Ph. Lambin, and J.-P. Vigneron for discussions and J.-M. Beuken for permanent computer assistance. Two of the authors (J.-C.C and X.G.) have benefited from the financial support of the National Fund for Scientific Research (Belgium). This paper presents research results of the Belgian Program on Interuniversity Attraction Poles initiated by the Belgian State, Prime Minister's Office, Science Policy Programming. We also acknowledge the use of the IBM-3090 of the Calculation Center of Louvain-La-Neuve and the RS 6000 work station of the PCPM, common projects between IBM Belgium and the Catholic University of Louvain-La-Neuve (UCL).

REFERENCES

1. J. D. Bernal, *Proc. R. Soc. London*, Ser. A **160,** 749 (1924).
2. H. Lipson and A. R. Stokes, *Proc. R. Soc. London*, Ser. A **181,** 101 (1942).
3. R. R. Haering, *Can. J. Phys.* **36,** 352 (1958).
4. L. Samuelson, I. P. Batra, and C. Roetti, *Solid State Comm.* **33,** 817 (1980); L. Samuelson and I. P. Batra, *J. Phys.* C **13,** 5105 (1980).
5. A. W. Moore, In *Highly Oriented Pyrolytic Graphite* (Edited by P. L. Walker, Jr., and P. A. Thrower, Chemistry and Physics of Carbon), Vol. 11, Marcel Dekker, New York (1965).
6. A. Marchand, In *Les Carbones* (Edited by A. Pacault, Masson), T. 1, Part. 3, pp 232–247, Masson & Cie, Paris (1965).
7. See references in M. S. Dresselhauss, G. Dresselhaus, K. Sugihara, I. L. Spain, and H. A. Goldberg, In *Graphite Fibers and Filaments* (Edited by Springer-Verlag, Springer Series in Materials Science), Vol. 5, Berlin (1988); N. B. Brandt, S. M. Chudinov, and Ya. G. Ponomarev, In *Semimetals: Graphite and its compounds* (Edited by North-Holland, Modern Problems in condensed Matter Sciences) Vol. 20.1, Amsterdam (1988).
8. P. R. Wallace, *Phys. Rev.* **71,** 622 (1947).
9. J. C. Slonczewski and P. R. Weiss, *Phys. Rev.* **99,** 636 (1955); J. C. Slonczewski, and P. R. Weiss, *Phys. Rev.* **109,** 272 (1958).
10. J. W. McClure, *Phys. Rev.* **108,** 612 (1957).
11. As the sign of the γ_2 parameter governs the nature of the carrier in the different pockets of the Fermi surface of hexagonal graphite, the positive value for γ_2 chosen by McClure entails an exchange of the nature of the carrier in his Fermi surface model in comparison with modern studies.
12. J. W. McClure, *Carbon* **7,** 425 (1969).
13. G. Dresselhaus and M. S. Dresselhaus, *Phys. Rev.* A**140,** 401 (1965).
14. F. Bassani and G. Pastori Parravicini, *Nuovo Cimento* B **50,** 95 (1967).
15. G. S. Painter and D. E. Ellis, *Phys. Rev.* B **1,** 4747 (1970); H. Nagayoshi, K. Nakao, and Y. Uemura, *Solid State Comm.* **18,** 225 (1976); R. C. Tatar and S. Rabii, *Phys. Rev.* B **25,** 4126 (1982); N. A. Holzwarth, S. G. Louie, and S. Rabii, *Phys. Rev.* B **26,** 5382 (1982); M. Posternak, A. Baldereschi, A. J. Freeman, E. Wimmer and M. Weinert, *Phys. Rev. Lett.* **50,** 761 (1983); H. J. F. Jansen and A. J. Freeman, *Phys. Rev.* B **35,** 8207 (1987); D. Tomanek, R. M. Wentzcovitch, S. G. Louie, and M. L. Cohen, *Phys. Rev.* B **37,** 3134 (1988).
16. A. Zunger, *Phys. Rev.* B **17,** 626 (1978); M. Weinert, E. Wimmer, and A. J. Freeman, *Phys. Rev.* B **26,** 4571 (1982).
17. D. P. DiVincenzo, E. J. Mele, and N. A. W. Holzwarth, *Phys. Rev.* B **27,** 2458 (1983); M. T. Yin and M. L. Cohen, *Phys. Rev.* B **29,** 6993 (1984).
18. S. Fahy, S. G. Louie, and M. L. Cohen, *Phys. Rev.* B **34,** 1191 (1986).
19. S. Fahy, S. G. Louie, and M. L. Cohen, *Phys. Rev.* B **35,** 7623 (1987).
20. J.-C. Charlier, X. Gonze and J.-P. Michenaud, *Phys. Rev.* B **43,** 4579 (1991).
21. J.-C. Charlier, J.-P. Michenaud, and X. Gonze, *Phys. Rev.* B **46,** 4531 (1992).
22. M. C. Schabel and J. L. Martins, *Phys. Rev.* B **46,** 7185 (1992).
23. J.-C. Charlier, J.-P. Michenaud, and Ph. Lambin, *Phys. Rev.* B **46,** 4540 (1992).
24. Ph. Lambin, J.-C. Charlier, and J.-P. Michenaud, submitted to Computational Materials Science (1993).
25. P. Hohenberg and W. Kohn, *Phys. Rev.* B **136,** 864 (1964); W. Kohn and L. J. Sham, *Phys. Rev.* A **140,** 1133 (1965).
26. D. M. Ceperley and B. J. Alder, *Phys. Rev. Lett.* **45,** 566 (1980); J. Perdew and A. Zunger, *Phys. Rev.* B **23,** 5048 (1981).
27. G. B. Bachelet, D. R. Hamann, and M. Schlüter, *Phys. Rev.* B **26,** 4199 (1982).
28. J. Ihm, A. Zunger, and M. L. Cohen, *J. Phys.* C **12,** 4409 (1979).
29. D. M. Wood and A. Zunger, *J. Phys.* A **18,** 1343 (1985).
30. P. H. Dederichs and R. Zeller, *Phys. Rev.* B **28,** 5462 (1983).
31. H. J. Monkhorst and J. D. Pack, *Phys. Rev.* B **13,** 5188 (1976).
32. Y. Baskin and L. Mayer, *Phys. Rev.* **100,** 544 (1955).

33. J.–C. Charlier, X. Gonze, and J.–P. Michenaud, in preparation.
34. M. Lax, *Symmetry Principles in Solid State and Molecular Physics*, pp. 308–311, Wiley, New York (1974).
35. G. Lehmann and M. Taut, *Phys. Stat. Sol.* (b) **54,** 469 (1972); Ph. Lambin and J.–P. Vigneron, *Phys. Rev.* B **29,** 3430 (1984) and references therein.
36. M. H. Boon, M. S. Methfessel, and F. M. Mueller, *J. Phys.* C **19,** 5337 (1986).
37. D. E. Soule, J. W. McClure, and L. B. Smith, *Phys. Rev.* A **134,** 453 (1964).
38. S. B. Trickey, F. Müller–Plathe, G. H. F. Diercksen, and J. C. Boettger, *Phys. Rev.* B **45,** 4460 (1992).
39. J.–C. Charlier, J.–P. Michenaud, X. Gonze, and J.–P. Vigneron, *Phys. Rev.* B **44,** 13237 (1991).
40. S. Fahy, private communication (Namur, 1993).
41. V. Bayot, L. Piraux, J.–P. Michenaud, J.–P. Issi, M. Lelaurain, and A. Moore, *Phys. Rev.* B **41,** 11770 (1990).
42. L. P. Bouckaert, R. Smoluchowski, and E. Wigner, *Phys. Rev.* **50,** 58 (1936).